

Quantum enhanced beam tracking surpassing the Heisenberg uncertainty limit

Yingwen Zhang,^{1,2,3,*} Duncan England,² Noah Lupu-Gladstein,² Frédéric Bouchard,²
Guillaume Thekkadath,² Philip J. Bustard,² Ebrahim Karimi,^{1,2,3} and Benjamin Sussman^{2,1,3}

¹*Nexus for Quantum Technologies, University of Ottawa, Ottawa ON Canada, K1N6N5*

²*National Research Council of Canada, 100 Sussex Drive, Ottawa ON Canada, K1A0R6*

³*Joint Centre for Extreme Photonics, National Research Council and University of Ottawa, Ottawa, Ontario, Canada*

Determining a beam's full trajectory requires tracking both its position and momentum (angular) information. However, the product of position and momentum uncertainty in a simultaneous measurement of the two parameters is bound by the Heisenberg uncertainty limit (HUL). In this work, we present a proof-of-principle demonstration of a quantum-enhanced beam tracking technique, leveraging the inherent position and momentum entanglement between photons produced via spontaneous parametric down-conversion (SPDC). We show that quantum entanglement can be exploited to achieve a beam tracking accuracy beyond the HUL in a simultaneous measurement. Moreover, with existing detection technologies, it is already possible to achieve near real-time beam tracking capabilities at the single-photon level. The technique also exhibits high resilience to background influences, with negligible reduction in tracking accuracy even when subjected to a disruptive beam that is significantly brighter than SPDC.

Beam tracking plays a crucial role in various technological and scientific applications, ranging from optical communications and remote sensing to high-precision imaging and laser-guided systems. Accurately determining a beam's full trajectory requires tracking both its position and momentum (angular) information. When using a coherent laser beam, the measurement accuracy is fundamentally bounded by the shot noise limit (SNL) when measuring each parameter, and when measuring both parameters simultaneously, the product of the uncertainties is bounded by the Heisenberg uncertainty limit (HUL).

Many studies have been conducted to beat classical measurement limits by using specific quantum states of light in sensing applications [1] such as quantum metrology [2, 3] and quantum imaging [4–6]. In the field of beam tracking, spatially squeezed light has been proposed and demonstrated as a method to surpass the SNL [7–9]. Furthermore, theoretical studies have explored the use of the spatial correlations inherent to entangled photons to beat both the SNL [10] and the HUL [11, 12]. It has also been theoretically shown that the quantum Cramér-Rao bound for beam displacement can be achieved using two-photon interference with spatial correlations [13].

In this work, we experimentally demonstrate quantum correlation beam tracking (QCBT) in which position and momentum entangled of photon pairs, produced through spontaneous parametric down-conversion (SPDC), is used to track a beam's trajectory. By making joint measurements on a pair of entangled photons, it is possible to measure correlations with a precision exceeding the HUL. This has been realized in both the position-momentum basis [14–18], and the time-frequency basis [19]. This property has been used as a gauge for entanglement. Here, we use this quantum property in the application of beam tracking, we show that QCBT

can potentially achieve an accuracy beyond the HUL, and can already be performed with current technology at a speed of ~ 1 Hz with an accuracy of $5 \mu\text{m}$ through just 100 correlated photons. Additionally, QCBT is extremely resilient to background influences as a result of the inherent temporal and spatial correlations between the SPDC photons.

To track the full trajectory of a light beam, the change in the beam location will need to be measured simultaneously in two different planes to determine both the position and momentum information. When using a camera-type detector to measure the beam in the position space $\mathbf{r} = (x, y)$ or the momentum space $\mathbf{k} = (u, v)$, the beam location is commonly determined via a centre-of-mass equation

$$\bar{\mathbf{r}} = \frac{\sum_{j=1}^{N_s} \mathbf{r}_j}{N_s}, \quad (1)$$

with N_s the total number of detected photons and \mathbf{r}_j the position where each photon is detected. This is the most optimal estimator of the beam centroid and the variance of the centroid in position is given by (see the Supplementary Materials for derivation)

$$\text{Var}(\bar{\mathbf{r}}) = \frac{\sigma_r^2}{N_s}, \quad (2)$$

with σ_r being the root-mean-squared width of the beam spot (assuming circular symmetry). Note that the above variance does not take into account the effect of the pixel size, a more thorough analysis taking this into account can be found in [20].

Thus, the variance in measuring a displacement from position \mathbf{r}_1 to \mathbf{r}_2 is given by:

$$\text{Var}(\Delta\bar{\mathbf{r}}) = \text{Var}(\bar{\mathbf{r}}_1) + \text{Var}(\bar{\mathbf{r}}_2) = \frac{2}{N_s} \sigma_r^2, \quad (3)$$

where we have assumed that the beam width and total number of photon detections for estimating $\langle \bar{\mathbf{r}}_1 \rangle$ and $\langle \bar{\mathbf{r}}_2 \rangle$,

* yzhang6@uottawa.ca

are approximately equal under the same data acquisition time. Equation (3) also applies to the Fourier plane, which gives the variance in the momentum, providing directional information.

Limited by the HUL, the product of the beam width in the position σ_r and momentum plane σ_k is

$$\sigma_r(\hbar\sigma_k) \geq \hbar/2. \quad (4)$$

As such, the uncertainty product in the change of position and momentum have the following bound

$$\sqrt{\text{Var}(\Delta\bar{\mathbf{r}})\text{Var}(\Delta\bar{\mathbf{k}})} = \frac{2}{N_s}\sigma_r\sigma_k \geq \frac{1}{N_s}. \quad (5)$$

Now we will show that by making joint measurements on a pairs of position-momentum entangled photons, it is possible to achieve an uncertainty product in the change of position and momentum with a precision exceeding this bound.

In the low gain regime, the position-momentum entangled state of SPDC in transverse momentum space can be written as

$$|\Psi\rangle = \int \int \phi(\mathbf{k}_s, \mathbf{k}_i) |\mathbf{k}_s, \mathbf{k}_i\rangle d^2k_s d^2k_i, \quad (6)$$

and the biphoton wavefunction $\phi(\mathbf{k}_s, \mathbf{k}_i)$ under a double-Gaussian approximation is given by [21–23]

$$\begin{aligned} \phi(\mathbf{k}_s, \mathbf{k}_i) \approx & A_k \exp\left(\frac{-\delta_r^2 |\mathbf{k}_s - \mathbf{k}_i|^2}{8}\right) \\ & \times \exp\left(\frac{-|\mathbf{k}_s + \mathbf{k}_i|^2}{2\delta_k^2}\right), \end{aligned} \quad (7)$$

where A_k is a normalization constant, $\delta_k \approx (1/2)\sigma_p$ with σ_p being the pump beam width and $\delta_r \approx \sqrt{\frac{2\alpha L\lambda_p}{\pi}}$ where L is the crystal length, λ_p is the pump wavelength, and $\alpha = 0.455$ is a constant factor from the Gaussian approximation of the sinc phase matching function [22].

Inverse Fourier transforming to position space, the biphoton wavefunction is then

$$\begin{aligned} \psi(\mathbf{r}_s, \mathbf{r}_i) \approx & A_r \exp\left(\frac{-|\mathbf{r}_s - \mathbf{r}_i|^2}{2\delta_r^2}\right) \\ & \times \exp(-2\delta_k^2 |\mathbf{r}_s + \mathbf{r}_i|^2). \end{aligned} \quad (8)$$

From Eqs. (7) and (8), we can see that the width of position correlation $\mathbf{r}_s - \mathbf{r}_i$ is δ_r and for the transverse momentum correlation $\mathbf{k}_s + \mathbf{k}_i$ width is δ_k . Utilizing these correlation measurements allows us to express the variance in the relative position and momentum as:

$$\begin{aligned} \text{Var}(\Delta\bar{\mathbf{r}}) &= \frac{\Delta|\mathbf{r}_s - \mathbf{r}_i|}{\sqrt{N_c}} = \sqrt{\frac{2}{N_c}}\delta_r, \\ \text{Var}(\Delta\bar{\mathbf{k}}) &= \frac{\Delta|\mathbf{k}_s + \mathbf{k}_i|}{\sqrt{N_c}} = \sqrt{\frac{2}{N_c}}\delta_k, \end{aligned} \quad (9)$$

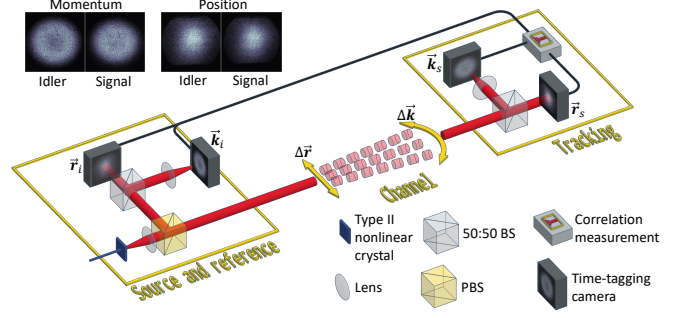


FIG. 1. Conceptual setup for quantum correlation beam tracking: In the ‘Source and reference’, position-momentum entangled photon pairs with orthogonal polarization are created through Type-II SPDC. One photon of the pair is split off using a PBS and then probabilistically split into being locally detected either in the position-plane or the momentum-plane of the non-linear crystal by time-tagging cameras. The other photon is sent through a ‘Channel’ whose stability needs to be monitored. In the ‘Tracking’ part of the setup, the photon is also probabilistically split into being detected in either the near or far field of the non-linear crystal by time-tagging cameras. A change in the trajectory of the signal photon beam is then tracked through displacements in the position and momentum correlation between the two photons. Typical images captured by the camera of the two planes for the photon pairs are shown on the top left.

where N_c is the number of detected photon pairs. The position-momentum uncertainty relation in Eq. (5) then becomes

$$\sqrt{\text{Var}(\Delta\bar{\mathbf{r}})\text{Var}(\Delta\bar{\mathbf{k}})} = \frac{2}{N_c}\delta_r\delta_k \quad (10)$$

Thus, if the product $\delta_r\delta_k < 1/2$, then the precision in measuring a change in beam trajectory can exceed the HUL.

A conceptual sketch of the setup used to realize QCBT is shown in Fig. 1. Position-momentum entangled photon pairs, known as the signal and idler photons, with orthogonal polarization are generated through Type-II SPDC. The photon pairs are then deterministically separated using a polarizing beam splitter (PBS) with the idler photons kept locally in a well-isolated system as a reference, while the signal photons are sent through a channel, which creates an unknown, time-varying, displacement on the beam. For detection, both photons are probabilistically split using a balanced beam splitter such that either the crystal’s position-plane (near-field) or the momentum-plane (far-field) is measured by time-tagging cameras, which can capture both the spatial and time-of-arrival information of the photons.

First, a time correlation measurement is performed between the two position-plane cameras and two momentum-plane cameras to identify photons that are detected in coincidence. Thereafter, a spatial correlation measurement is performed, whereby $\mathbf{r}_s - \mathbf{r}_i$ is determined from the photon pairs captured in the position-planes and

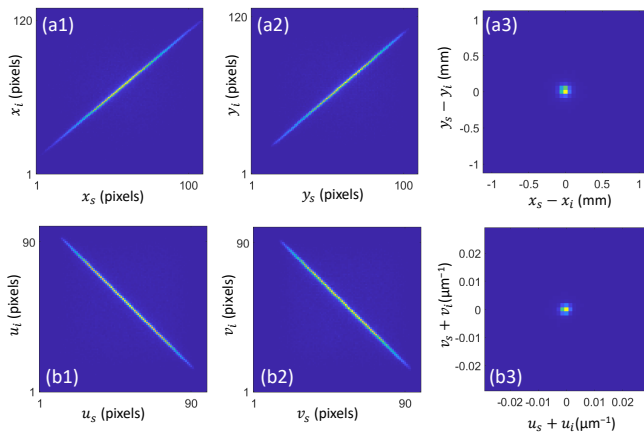


FIG. 2. **SPDC correlation in near- and far-field:** (a1, a2) Measured position correlation of SPDC photons in the x and y direction. The difference-coordinate projection of position correlation is shown in (a3). (b1, b2) Measured momentum anti-correlation of the SPDC photons in the u and v direction. The sum-coordinate projection of momentum anti-correlation is shown in (b3).

$\mathbf{k}_s + \mathbf{k}_i$ determined through pairs from the momentum-planes.

For this proof-of-concept demonstration, we used a single camera (TPX3CAM [24, 25]) to capture both the signal and idler photons in the position and momentum plane instead of measuring them separately with multiple cameras. A mirror mounted on a motorized translation stage placed in between the two planes acts as the unknown channel and provides a simultaneous beam displacement in both planes. Results from using the spatial correlations of SPDC photon pairs are compared to a coherent laser where the beam is tracked through a single photon on the signal beam arm. More details on the experimental setup can be found in the Supplementary Materials.

The measured spatial correlations of SPDC at the camera plane is shown in Fig. 2. When a Gaussian is fitted, a width of $\delta_r = 42 \pm 2 \mu\text{m}$ (0.76 pixels) is obtained for the $\mathbf{r}_s - \mathbf{r}_i$ profile, and $\delta_k = (1.06 \pm 0.04) \times 10^{-3} \mu\text{m}^{-1}$ (0.74 pixels) for the $\mathbf{k}_s + \mathbf{k}_i$ profile. This would give a position-momentum uncertainty product of $(0.088 \pm 0.005)/N$, indicating that a measurement precision beyond the HUL should be possible. For the laser beam we have $\sigma_r = 52.7 \pm 0.7 \mu\text{m}$ and $\sigma_k = (1.41 \pm 0.02) \times 10^{-2} \mu\text{m}^{-1}$, giving an uncertainty product of $(1.49 \pm 0.03)/N$, thus not surpassing the HUL.

Figure 3 shows the experimental results of beam tracking with the two light sources. Figure 3(a) shows the uncertainty product for the two sources as a function of the number of detected events N . The average uncertainty product, determined through 50 repeated measurements at each N , are $(0.114 \pm 0.005)/N$ and $(1.54 \pm 0.04)/N$ for the correlated SPDC and laser, respectively.

In Fig. 3(b) we translate a mirror by various distances and compare the measured displacement in the

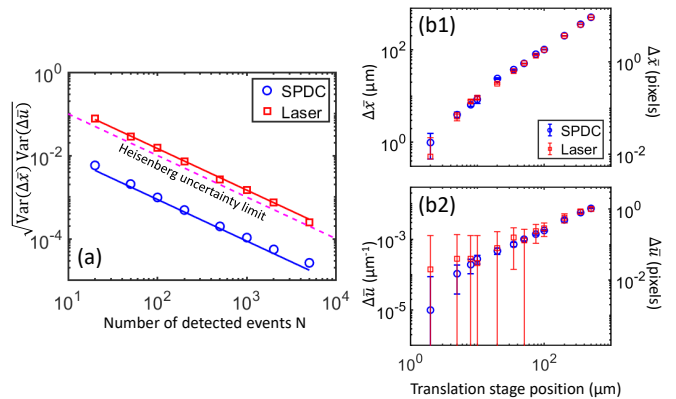


FIG. 3. **Beam tracking accuracy:** (a) Position-momentum uncertainty product for the change in beam trajectory as a function of the number of detected events. This is compared for the cases of using the spatial correlations of SPDC (blue circles) and a laser (red squares). The solid lines are the expected uncertainty product based on the measured correlation and beam widths. The purple dashed line is the HUL corresponding to $\sqrt{\text{Var}(\Delta\bar{\mathbf{r}})\text{Var}(\Delta\bar{\mathbf{k}})} = 1/N$. (b1, b2) compares the measured beam displacement in the position and momentum planes for $N = 5000$ while using SPDC spatial correlations (blue circles) and a laser (red squares).

position (Fig. 3(b1)) and momentum (Fig. 3(b2)) plane for the laser and the correlated SPDC. This is measured at $N = 5000$ with uncertainty obtained through 50 repeated measurements. Note that the mirror translates the beam horizontally, so position (momentum) shifts are only measured in the x (u) direction. In the position plane (Δx), SPDC achieves comparable uncertainty to the laser since $\delta_r \simeq \sigma_r$. However, in the momentum plane (Δu), the SPDC offers far smaller uncertainty since $\delta_k \ll \sigma_k$: this is a direct visualization of the advantage of using entangled light for beam tracking.

It is important to note that a detection event is defined differently for different light sources. For the laser, this is the detection of a single photon on one of the tracking cameras, so $N = N_s$. For the correlated SPDC measurement, this is the coincident detection of a signal and an idler photon, thus $N = N_c$. For realistic detectors, N_s and N_c are related by $N_c = \epsilon_i N_s$ where $\epsilon_i \leq 1$ is the detection efficiency of the idler photons. In this case, the HUL bound of Eq. (10) is modified into

$$\sqrt{\text{Var}(\Delta\bar{\mathbf{r}})\text{Var}(\Delta\bar{\mathbf{k}})} = \frac{2\delta_r\delta_k}{\epsilon_i N_s}. \quad (11)$$

Thus, unconditionally beating the HUL will require $\epsilon_i > 2\delta_r\delta_k$, which for our demonstration ϵ_i must be greater than 0.11. Unfortunately for this experimental system, $\epsilon_i \approx 0.02$, which takes into account the camera detection efficiency of ~ 0.08 [26], losses in the system, and statistically splitting the photons between the position and momentum planes which accounts for a 50% loss in the spatial-temporal correlated events.

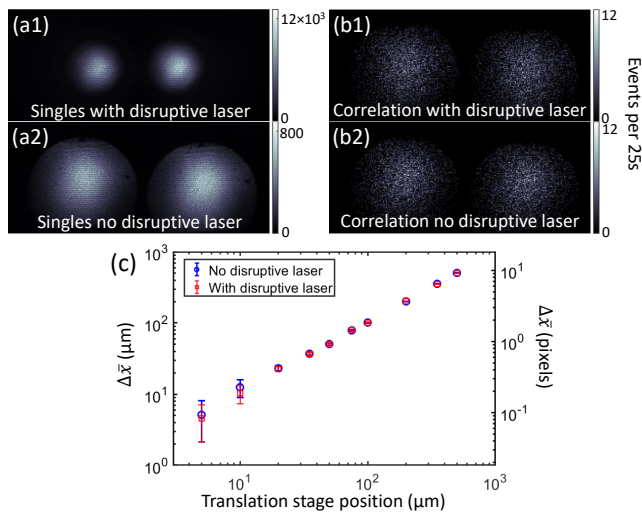


FIG. 4. **Beam tracking accuracy under a strong background:** (a1, a2) Image from just singles events of the SPDC light with and without a bright disruption laser applied. (b1, b2) Detected temporally and spatially correlated photons with and without the disruption laser being applied. (c) Comparing the measured beam displacement from 1000 correlated events for QCBT with and without the disruption laser. Uncertainties are determined through 50 repeated measurements

In addition to using a higher efficiency camera to improve ϵ_i , one can try to circumvent the need to statistically split the photons by modifying the time-tagging camera into a light-field camera [27, 28], enabling simultaneous measurement of position and momentum information of the photons. One can also design the SPDC source to have smaller δ_r and δ_k to reduce the required ϵ_i . However, both approaches require that the time-tagging camera have a higher spatial resolution than that available here. With the rapid advance of single-photon camera technologies [29, 30], we expect that a time-tagging camera with enough efficiency and resolution to unconditionally beat the HUL will be available in the near future.

We also demonstrate that it is now possible to perform real-time measurements of the temporal-spatial correlations of SPDC and use this for beam tracking through

QCBT. Using an Intel Xeon W-2145 CPU, we can process the temporal and spatial correlation of around 10^5 detection events per second resulting in ~ 100 correlated events in both the position and momentum planes. This allows tracking of the beam displacement with an accuracy of $\sim 5 \mu\text{m}$ (0.1 pixels). This is shown in the Supplementary Video. With the latest generation of CPUs or possibly with GPU processing, we expect the speed of data processing can be significantly improved, allowing for faster tracking speed and higher accuracy. Details on TPX3CAM data processing can be found in [26, 31].

Beam tracking can be very sensitive to background influences; any incomplete background removal will lead to an incorrect centroid measurement. QCBT exhibits extreme background tolerance through the time and spatial correlation of SPDC photons. Here a disruptive laser beam that has approximately 10 times more photons than SPDC is applied on both the signal and idler regions of the camera as seen in Fig, 4(a). After post-selecting on temporally and spatially correlated photons, we can see in Fig, 4(b) that the disruptive laser beam is completely removed. The result of beam tracking in the position plane comparing the cases of having the disruptive laser beam on or off is shown in Fig, 4(c). The two scenarios show perfect agreement in the measured beam displacement with no statistically significant changes in the measurement uncertainties.

In conclusion, we have demonstrated a proof-of-principle quantum enhanced beam tracking technique using position-momentum entangled SPDC photons and have shown how it can be used to achieve a beam tracking accuracy beyond the bound of the HUL. Assuming perfect detectors, QCBT with our system can achieve a position-momentum uncertainty product of $0.11/N$ compared to the HUL bound of $1/N$. We also demonstrate real-time beam tracking using QCBT at a speed of ~ 1 Hz with an accuracy of $5 \mu\text{m}$ through just 100 correlated photons. QCBT is also extremely resistant to background influences; we show that even when a disruptive laser that is ten times brighter than SPDC is applied, there is still negligible effect on the accuracy of QCBT. This type of tracking system will be desirable for stabilizing low-brightness quantum channels for applications such as quantum communications and quantum remote sensing.

[1] S. Pirandola, B. R. Bardhan, T. Gehring, C. Weedbrook, and S. Lloyd, Advances in photonic quantum sensing, *Nature Photonics* **12**, 724 (2018).
 [2] E. Polino, M. Valeri, N. Spagnolo, and F. Sciarrino, Photonic quantum metrology, *AVS Quantum Science* **2**, 024703 (2020).
 [3] M. Barbieri, Optical quantum metrology, *PRX Quantum* **3**, 010202 (2022).
 [4] P.-A. Moreau, E. Toninelli, T. Gregory, and M. J. Padgett, Imaging with quantum states of light, *Nature Reviews Physics* **1**, 367 (2019).

[5] O. S. Magaña-Loaiza and R. W. Boyd, Quantum imaging and information, *Reports on Progress in Physics* **82**, 124401 (2019).
 [6] H. Defienne, W. P. Bowen, M. Chekhova, G. B. Lemos, D. Oron, S. Ramelow, N. Treps, and D. Faccio, Advances in quantum imaging, *Nature Photonics* **18**, 1024 (2024).
 [7] C. Fabre, J. B. Fouet, and A. Maître, Quantum limits in the measurement of very small displacements in optical images, *Opt. Lett.* **25**, 76 (2000).
 [8] N. Treps, U. Andersen, B. Buchler, P. K. Lam, A. Maître, H.-A. Bachor, and C. Fabre, Surpassing the standard

- quantum limit for optical imaging using nonclassical multimode light, *Phys. Rev. Lett.* **88**, 203601 (2002).
- [9] N. Treps, N. Grosse, W. P. Bowen, C. Fabre, H.-A. Bachor, and P. K. Lam, A quantum laser pointer, *Science* **301**, 940 (2003).
- [10] K. Lyons, S. Pang, P. G. Kwiat, and A. N. Jordan, Precision optical displacement measurements using biphotons, *Phys. Rev. A* **93**, 043841 (2016).
- [11] A. Di Lorenzo, Correlations between detectors allow violation of the heisenberg noise-disturbance principle for position and momentum measurements, *Phys. Rev. Lett.* **110**, 120403 (2013).
- [12] T. J. Bullock and P. Busch, Focusing in arthurs-kelly-type joint measurements with correlated probes, *Phys. Rev. Lett.* **113**, 120401 (2014).
- [13] D. Triggiani and V. Tamma, Estimation with ultimate quantum precision of the transverse displacement between two photons via two-photon interference sampling measurements, *Phys. Rev. Lett.* **132**, 180802 (2024).
- [14] Y.-H. Kim and Y. Shih, Experimental realization of popper's experiment: Violation of the uncertainty principle?, *Foundations of Physics* **29**, 1849 (1999).
- [15] J. C. Howell, R. S. Bennink, S. J. Bentley, and R. W. Boyd, Realization of the einstein-podolsky-rosen paradox using momentum- and position-entangled photons from spontaneous parametric down conversion, *Phys. Rev. Lett.* **92**, 210403 (2004).
- [16] M. P. Edgar, D. S. Tasca, F. Izdebski, R. E. Warburton, J. Leach, M. Agnew, G. S. Buller, R. W. Boyd, and M. J. Padgett, Imaging high-dimensional spatial entanglement with a camera, *Nature Communications* **3**, 984 (2012).
- [17] P.-A. Moreau, F. Devaux, and E. Lantz, Einstein-podolsky-rosen paradox in twin images, *Phys. Rev. Lett.* **113**, 160401 (2014).
- [18] B. Ndagano, H. Defienne, A. Lyons, I. Starshynov, F. Villa, S. Tisa, and D. Faccio, Imaging and certifying high-dimensional entanglement with a single-photon avalanche diode camera, *npj Quantum Information* **6**, 94 (2020).
- [19] J.-P. W. MacLean, J. M. Donohue, and K. J. Resch, Direct characterization of ultrafast energy-time entangled photon pairs, *Phys. Rev. Lett.* **120**, 053601 (2018).
- [20] H. Jia, J. Yang, and X. Li, Minimum variance unbiased subpixel centroid estimation of point image limited by photon shot noise, *J. Opt. Soc. Am. A* **27**, 2038 (2010).
- [21] C. K. Law and J. H. Eberly, Analysis and interpretation of high transverse entanglement in optical parametric down conversion, *Phys. Rev. Lett.* **92**, 127903 (2004).
- [22] K. W. Chan, J. P. Torres, and J. H. Eberly, Transverse entanglement migration in hilbert space, *Phys. Rev. A* **75**, 050101 (2007).
- [23] J. Schneeloch and J. C. Howell, Introduction to the transverse spatial correlations in spontaneous parametric down-conversion through the biphoton birth zone, *Journal of Optics* **18**, 053501 (2016).
- [24] A. Nomerotski, Imaging and time stamping of photons with nanosecond resolution in timepix based optical cameras, *Nuclear Instruments and Methods in Physics Research Section A: Accelerators, Spectrometers, Detectors and Associated Equipment* **937**, 26 (2019).
- [25] <https://www.amscins.com/product/chronos-series/phoebe/> ().
- [26] V. Vidyapin, Y. Zhang, D. England, and B. Sussman, Characterisation of a single photon event camera for quantum imaging, *Scientific Reports* **13**, 1009 (2023).
- [27] X. Xiao, B. Javidi, M. Martínez-Corral, and A. Stern, Advances in three-dimensional integral imaging: sensing, display, and applications, *Appl. Opt.* **52**, 546 (2013).
- [28] M. Martínez-Corral and B. Javidi, Fundamentals of 3d imaging and displays: a tutorial on integral imaging, light-field, and plenoptic systems, *Adv. Opt. Photon.* **10**, 512 (2018).
- [29] <https://www.amscins.com/product/cheetah-series/> ().
- [30] <https://global.canon/en/technology/spad-sensor-2023.html>.
- [31] A. Zhao, M. van Beuzekom, B. Bouwens, D. Byelov, I. Chakaberia, C. Cheng, E. Maddox, A. Nomerotski, P. Svihra, J. Visser, V. Vrba, and T. Weinacht, Coincidence velocity map imaging using tpx3cam, a time stamping optical camera with 1.5 ns timing resolution, *Review of Scientific Instruments* **88**, 113104 (2017).

Acknowledgment: The authors are grateful to Aaron Goldberg for stimulating discussion. This work was supported by NRC-uOttawa Joint Centre for Extreme Quantum Photonics (JCEP) via the Quantum Sensors Challenge Program at the National Research Council of Canada, Quantum Enhanced Sensing and Imaging (QuEnSI) Alliance Consortia Quantum grant, and the Canada Research Chair (CRC) Program.

I. SUPPLEMENTARY MATERIALS

A. Details on the experimental setup

The experimental setup demonstrating QCBT is shown in Fig. 5(a). Position-momentum entangled photon pairs with orthogonal polarization are generated by pumping a 1 mm thick Type-II ppKTP crystal with a 405 nm CW laser. The two photons are first separated using a PBS and then, using HWPs, the polarization of each photon is rotated by $\pi/4$ so at the second PBS each photon will have a 50% probability of being imaged either at the position-plane of the crystal or the momentum-plane of the crystal. To create a beam displacement, a mirror mounted on a motorized translation stage is placed in between the crystal's position and momentum planes. The photon trajectories are slightly misaligned after the second PBS such that their trajectories are not perfectly parallel to each other; this way, moving the mirror will cause a simultaneous displacement of the beam in both the position and momentum planes.

For comparison of QCBT with the best classical scenario, the setup can be switched between using a SPDC source or an attenuated 810 nm laser by a flip mirror. The time-tagging camera used for detection is the TPX3CAM which has a resolution of 256×256 pixels with a pixel pitch of $55 \mu\text{m}$ and is able to time tag the photons detected on each pixel with ~ 7 ns accuracy. Typical images captured with the camera for the position and momentum planes of SPDC and laser are shown in Fig. 5(b).

The expected correlation widths can be approximated according to [22]:

$$\begin{aligned}\delta_k &\approx 1/2\sigma_p, \\ \delta_r &\approx \sqrt{\frac{2\alpha L\lambda_p}{\pi}}\end{aligned}\quad (12)$$

With the experimental parameters $L = 1$ mm, $\lambda_p = 405$ nm, $\sigma_p = 0.24$ mm and a $5 \times$ magnification in the imaging system from the crystal to the camera, we expect $\delta_r = 55 \mu\text{m}$ and $\delta_k = 0.82 \times 10^{-3} \mu\text{m}^{-1}$ at the camera. These values are in approximate agreement with the measured values of $\delta_r = 42 \mu\text{m}$ and $\delta_k = 1.1 \times 10^{-3} \mu\text{m}^{-1}$.

B. Optimal beam centroid estimator

To show that the center of mass equation

$$\bar{x} = \frac{\sum_{j=1}^N x_j}{N}, \quad (13)$$

is the most optimal estimator of the beam centroid x_c , we first note that \bar{x} is an unbiased estimator of x_c since

the expectation value of \bar{x}

$$\begin{aligned}E[\bar{x}] &= E\left[\frac{\sum_{j=1}^N x_j}{N}\right] \\ &= \frac{\sum_{j=1}^N E[x_j]}{N} \\ &= x_c.\end{aligned}\quad (14)$$

Secondly, we must show that \bar{x} saturates the Cramer-Rao bound

$$\text{Var}(\bar{x}) = \frac{1}{NI}, \quad (15)$$

where I is the Fisher information given by

$$I = E\left[\left(\frac{\partial}{\partial x_c} \log P(x|x_c, \sigma)\right)^2\right], \quad (16)$$

with $P(x|x_c, \sigma)$ the probability to detect a photon at position x given the beam's centroid x_c and a root-mean-squared waist $\sigma = \sqrt{\frac{\sum_{j=1}^N (x_j - \bar{x})^2}{N}} = \sqrt{\text{Var}(x_j)}$.

The variance $\text{Var}(\bar{x})$ is

$$\begin{aligned}\text{Var}(\bar{x}) &= \text{Var}\left(\frac{\sum_{j=1}^N x_j}{N}\right) \\ &= \frac{1}{N^2} \text{Var}\left(\sum_{j=1}^N x_j\right) \\ &= \frac{1}{N^2} \sum_{j=1}^N \text{Var}(x_j) \\ &= \frac{\sigma^2}{N},\end{aligned}\quad (17)$$

where in the 3rd line we have assumed that the photon positions x_i are independent.

Assuming a Gaussian distribution for $P(x|x_c, \sigma) = \frac{1}{\sqrt{2\pi\sigma^2}} \exp\left(-\frac{(x-x_c)^2}{2\sigma^2}\right)$,

$$\begin{aligned}I &= E\left[\left(\frac{\partial}{\partial x_c} \frac{-(x-x_c)^2}{2\sigma^2}\right)^2\right] \\ &= E\left[\frac{(x-x_c)^2}{\sigma^4}\right] \\ &= \frac{1}{\sigma^2},\end{aligned}\quad (18)$$

thus $1/NI = \sigma^2/N$, which is the variance given by Eq.17. This signifies that, when assuming a Gaussian probability distribution, the center of mass equation does satisfy the Cramer-Rao bound and is thus the most optimal beam centroid estimator.

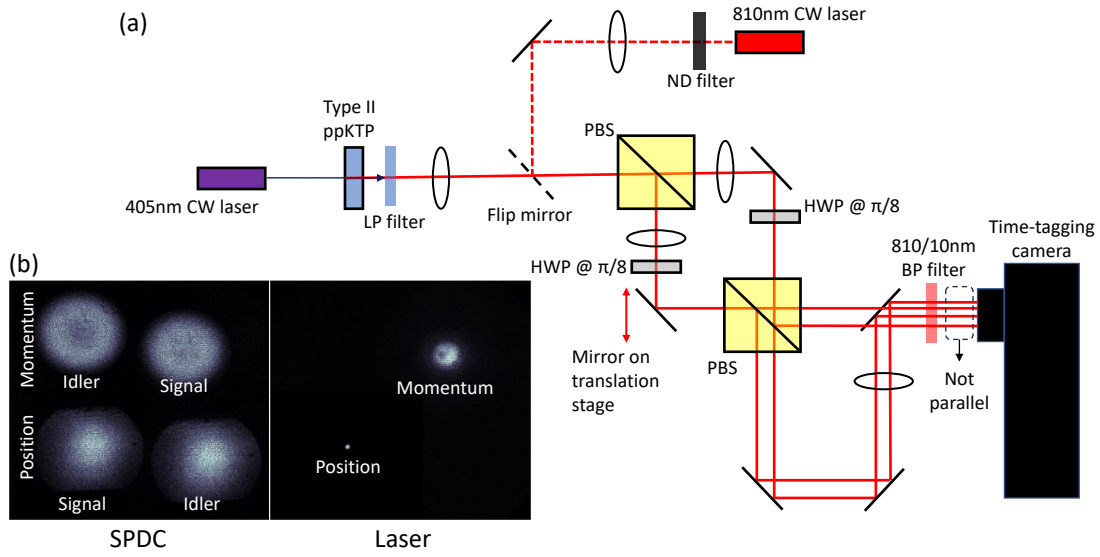


FIG. 5. **Experimental setup for SPDC beam tracking:** (a) Experimental setup for demonstrating QCBT. LP-filter: long-pass filter, BP-filter: band-pass filter, ND-filter: neutral density filter, PBS: polarizing beam-splitter, HWP: half-wave plate (b) Image captured on camera of the position and momentum planes from SPDC and laser. Note that in order to also see the laser momentum plane in the same image, the laser position plane intensity is displayed at 1/30 of the actual intensity.